Numerical simulation of bitumen emulsion-stabilised base course mixtures with C&D waste aggregates considering nonlinear elastic behaviour

Ignacio Pérez[a],, Luis Medina[a], Breixo Gómez-Meijide[b], Pedro Alves Costa[c], Antonio Silva Cardoso[c]*

[a]Universidade da Coruña. Department of Civil Engineering. E.T.S.I. Caminos, Canales y Puertos, Campus de Elviña s/n, 15071. A Coruña, Spain
**Corresponding author. Tel.: +34-981167000. Fax: +34-981167170*
[b]European Asphalt Pavement Association. R. du Commerce 77, 1040 Brussels, Belgium
[c]Faculty of Engineering of the Universidade do Porto, R. Roberto Frias. Porto, Portugal
E-mail addresses: iperez@udc.es (I. Pérez); lmedina@udc.es (L. Medina); breixo@eapa.org (B. Gómez Meijide); pacosta@fe.up.pt (P.A. Costa); scardoso@fe.up.pt (A. S. Cardoso)

Abstract

This study presents the numerical modelling of a load-volume road pavement section with bitumen emulsion-stabilised base courses. The base courses used natural and construction and demolition aggregates. A 3D finite difference model was used to determine the peak responses of the pavement sections when subjected to loads. Three nonlinear models were adopted in the two base courses. The response predictions of the three models were similar. Both the resilient and permanent behaviours of these materials were modelled. An analysis was conducted on the rutting resistance of the base course materials. Both base courses were suitable for use in low-volume roads. The base course made with construction and demolition aggregates was more resistant to rutting.

Keywords: FLAC3D, bitumen emulsion, stabilised base course, C&D waste aggregates, rutting.

1. Introduction

Bitumen-stabilised materials with emulsion (BSM) are not only more environmentally friendly but also more economical than other types of asphalt mixtures such as hot-mix asphalt (HMA). Thus, these mixtures of aggregates, asphalt emulsion, and water, which can be mixed, stored, and transported at room temperature, are gaining importance in the field of road engineering as a tool to fight against climate change. Furthermore, the latest developments in cold asphalt technology have contributed to minimise classical problems such as their higher air-void content after compaction and weak early-life strength [1, 2]. Both the environmental and economic aspects can be enhanced by replacing natural aggregates (NAs) with recycled aggregates from construction and demolition waste (CDAs), in a similar way other publications have demonstrated for different road construction materials such as concrete [3, 4] and HMA [5, 6].

BSM materials exhibit a behaviour similar to both granular materials (stress dependency) and HMA (temperature and frequency of loading dependency) [7, 8]. According to Jenkins et al. [9] and Ebels [10], the nonlinear elastic behaviour tends to be highlighted at early curing stages after pavement construction, while the viscoelastic behaviour becomes more significant when the material is cured after a period of time that sometimes lasts several months or years.

According to some authors [9, 10, 11], the nonlinear behaviour of BSM materials makes the shear strength the most critical mechanical property. Consequently, the failure of BSM materials is principally the result of significant permanent deformation (rutting) with an irreversible effect on the structural and functional state of pavement. In this sense, Ebels [10] and Hornych et al. [12] studied the nonlinear behaviour of a BSM-type grave emulsion using triaxial tests. This behaviour was checked by Santagata et al. [13] with a short-term evaluation of the mechanical properties of BSMs. It was also studied in a laboratory by Gómez-Meijide and Pérez [14] for BSMs with NAs and CDAs by means of dynamic-load triaxial tests such as resilient modulus (M_r) and permanent deformation constant confining pressure (CCP) tests.

In this context, in most cases, the structural analysis of pavement with BSM layers is performed under the similar principles employed in pavement with HMA layers [15]. In this way, BSM materials are studied as elastic or viscoelastic materials [15]. For instance, Shanbara et al. [16] investigated the linear elastic behaviour of cold-mix asphalt using the finite element method to obtain deflections on the pavement. The authors also obtained the stress and strain distributions in a cold asphalt mix with a glass fibre and predicted the rutting behaviour of natural fibre-reinforced cold-mix asphalt using the finite element method taking into account the viscoelastic behaviour [17]. Nevertheless, a different way to proceed is to consider the nonlinear nature of BSM materials. In this regard, Pérez et al. [18] used the nonlinear parameters obtained by Ebels [10] to investigate the nonlinear performance of BSMs and determine that rutting is the main mechanism of failure in these materials and that they are suitable for use in light-traffic roads.

2. Aim and scope

In this study, the laboratory results of the nonlinear behaviour investigations performed by triaxial tests were translated into numerical simulations with a fast Lagrangian analysis of continua in three dimensions (FLAC3D) model. The model predict the real behaviour of a base course pavement section made with BSM materials in low-volume roads. In this regard, the responses at critical positions of the pavement layers and the cumulative permanent deformation (rutting) of the BSM layers were analysed.

The simulations were performed for BSM made with cured and uncured CDAs, and the results were compared with those obtained with a controlled mixture made purely with NA. The simulations were performed to demonstrate that BSMs made with NA and CDA have enough structural capacity to resist rutting in low-volume road pavement. A complementary objective was to determine if it was possible to use a CDA as a substitute for an NA and, if so, if any of the properties of the BSM materials were improved. This would contribute to sustainable construction, as CDAs would be valued.

3. Materials properties

3.1. BSM base-course properties

3.1.1. Gradation

A continuous gradation-type grave-emulsion aggregate (Fig. 1) was selected for the BSM base-course material as specified by the Spanish Technical Association of Bituminous Emulsions (ATEB) [19]. This gradation was suitable for medium- and low-traffic levels. In Spain, grave emulsion has been employed as a base-course layer with very good resistance to permanent deformation. In addition, it has been used as an anti-reflecting cracking layer, obtaining excellent results that place it above cement-treated layers.

3.1.2. Aggregates and bitumen emulsion properties

BSM materials with CDA were studied. The main part of the recycled aggregate was composed of concrete, mortar, and stone with a certain proportion of impurities such as ceramic, metal pieces, gypsum, plastic, and glass. All the tests were repeated with control mixes for comparison purposes. The aggregate of these mixes was a natural common metamorphic siliceous aggregate (NA) extracted from a local quarry in Ourense, Spain. The main characteristics of the NA and CDA are listed in Table 1.

The selected binder was C60B5GE, a cationic slow-setting bitumen emulsion (60% bitumen content) with a 100-pen-grade base bitumen that fulfilled the specifications of the UNE EN 13808 standard.

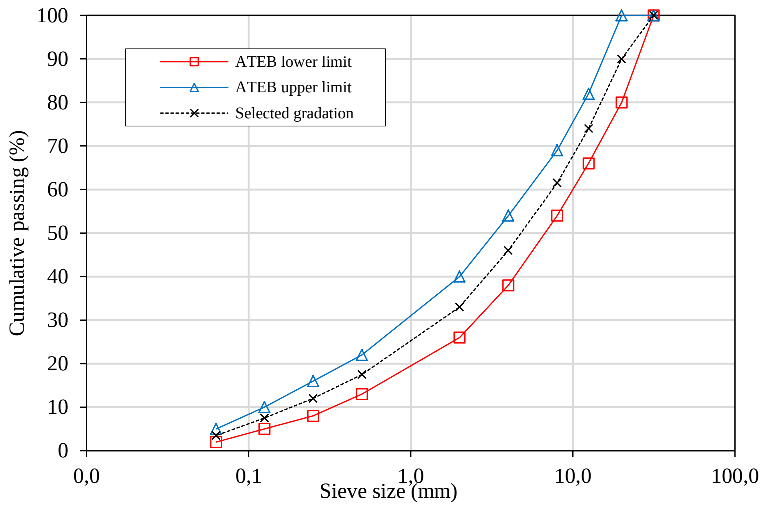

Fig. 1. BSM aggregate gradation with ATEB recommendation.

Table 1. Characterisation of CDA and NA aggregates [14]

Property	CDA	NA
Flakiness index (UNE EN 933-3)	4.5%	19.8%
Crushed particles (UNE EN 933-5)	89%	94%
Sand equivalent (UNE EN 933-8)	77%	78%
Los Angeles coefficient (UNE EN 1097-2)	38%	14%
Bulk specific gravity (UNE EN 1097-6)	2.64 t/m^3	2.78 t/m^3
Dry specific gravity (UNE EN 1097-6)	2.23 t/m^3	2.74 t/m^3
SSD specific gravity (UNE EN 1097-6)	2.39 t/m^3	2.75 t/m^3
Absorption coefficient (UNE EN 1097-6)	7.0%	0.5%

3.1.3. Preparation of samples

Optimum bitumen content and water content

The indirect tensile strength ratio (ITSR) test according to the Standard EN 12697-12 was used to determine the optimum bitumen and water contents. For the BSM made with NA, four series of 10 cylindrical samples each were manufactured with 3 % of water content and four different bitumen contents (2, 3, 4, and 5%). For the BSM made with CDA, four series of 10 cylindrical samples each were manufactured with 9 % of water content and four different bitumen contents (5, 6, 7, and 8%). The samples with CDAs needed a higher amount of water and bitumen because these aggregates have a very high absorption coefficient (Table 1). Five samples of each series were conditioned (wet group) and the other five samples remained at room temperature (dry group) according to EN 12697-12. Then, both groups of samples were subjected to the indirect tensile strength (ITS) tests according to the Standard EN 12697-23. Once the ITSR test results for the NA samples were analysed it was found that the optimum contents were 4% of bitumen and 3% of water (ITSR=79%; ITS_{dry}=851 kPa and ITS_{wet}=675 kPa). For the CDA the samples the optimum contents were 6% of bitumen and 9% of water (ITSR=70%; ITS_{dry}=862 kPa and ITS_{wet}=602 kPa). It was considered that ITSR≥70% are suitable for BSM base courses for medium- and low-traffic levels.

Final samples for resilient modulus test and permanent deformation test

Finally, for the resilient modulus and permanent deformation tests (Figure 2) the BSM samples were prepared with a diameter of 100 mm and a height of 200 mm with the two types of aggregates as published by Gómez-Meijide and Pérez [14]. All the samples with NA were manufactured with 3% water and 4% bitumen, and all the samples with CDA were manufactured with 9% water and 6% bitumen. After compaction some samples were testing immediately, and others were left to cure three days in an oven at 50 ºC before testing. According to the ATEB, the curing of the samples for three days is equivalent to a real highway in-situ curing period of six months [19].

3.1.4. Mechanical properties

Resilient modulus nonlinear models

A nonlinear elastic behaviour was adopted for the base layers of the BSM material. The specific weight, γ_{sat}, was 22.0 kN/m^3, and the coefficient of earth pressure at rest, K_0, was 0.6. The Poisson coefficient, ν, was 0.35. The nonlinear elastic behaviour was determined by dynamic load triaxial tests with CCP in accordance with the Standard EN 13286-7 recommendations as published by Gómez-Meijide and Pérez [14]. The test apparatus used consisted of a removable chamber and an axial-load system generator (Fig. 2). An independent air compressor was used to provide the confining pressure (maximum 10 bar), while a hydraulic system was used to control the axial load generator.

Three different resilient modulus (M_r) models were fitted to the experimental data. The models were the Hicks model (M_r-θ model) [20], Uzan model [21], and NCHRP model (proposed by the National Cooperative Highway Research Program) [22] described respectively as

$$M_r = k_1 \cdot \theta^{k_2}, \tag{1}$$

$$M_r = k_1 \cdot \theta^{k_2} \cdot {\sigma_d}^{k_3}, \tag{2}$$

$$\frac{M_r}{P_a} = k_1 \left(\frac{\theta}{P_a}\right)^{k_2} \left(\frac{\tau_{oct}}{P_a} + 1\right)^{k_3}, \tag{3}$$

where θ is the sum of the principal stresses or bulk stress ($\theta = \sigma_1 + 2\sigma_3$), σ_d is the deviator stress, τ_{oct} is the octahedral stress, P_a is a reference pressure (P_a = 101.35 kPa), and k_1, k_2, and k_3 are the material constants used for the FLAC3D numerical simulations.

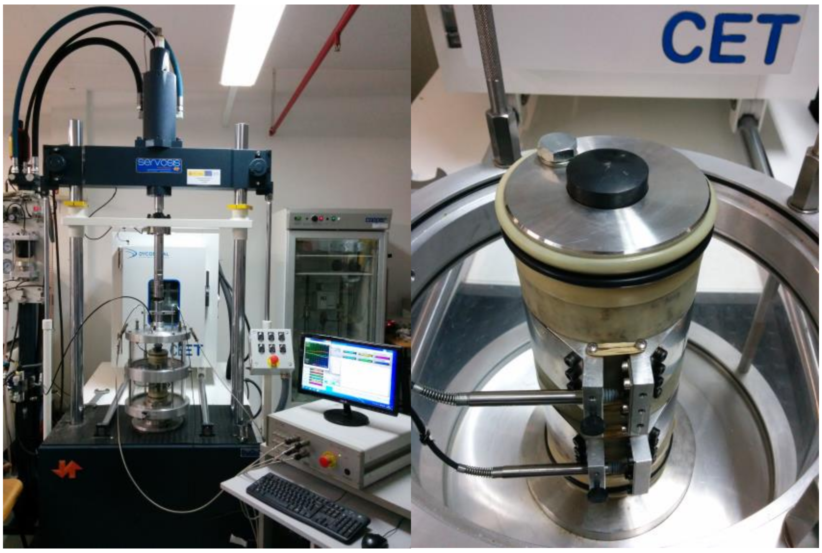

Fig. 2. Sample and sensor arrangement for resilient modulus triaxial test according to Standard EN 13286-7.

The model parameters of Gómez-Meijide and Pérez [14] were obtained by minimising the squared error between the models and the experimental moduli obtained in the laboratory. The coefficient values of the three models for CDAs and NAs are listed in Table 2.

Table 2. BSM nonlinear model coefficients [14]

Aggregate	Cured	Model: Hicks		Model: Uzan			Model: NCHRP		
		k_1	k_2	k_1	k_2	k_3	k_1	k_2	k_3
NA	yes	157.678	0.341	119.112	0.651	-0.302	7.765	0.550	-0.477
	no	16.132	0.596	11.583	1.033	-0.438	2.563	0.925	-0.721
CDA	yes	9.489	0.720	6.998	1.113	-0.393	2.664	1.087	-0.796
	no	9.755	0.636	7.469	0.990	-0.355	1.856	0.925	-0.633

As shown in Table 2, the cured and uncured BSM materials with NA had higher coefficient values. Therefore, BSM materials with NA are stiffer that BSM materials with CDA. In addition, BSM materials with NAs and CDAs are stiffer after curing.

Shear strength parameters

The shear strength parameters cohesion (*c*) and angle of friction (*φ*) were obtained by Gómez-Meijide and Pérez [14] by means of static triaxial tests (Table 3). Some authors [9, 10, 18] consider that *c* and *φ* determine the shear strength and therefore the resistance to permanent deformation of BSM materials. The results in Table 3 show that in both aggregates after curing, *c* and φ increased and improved the resistance to permanent deformation.

Table 3. Shear strength parameters [14]

Aggregate	Cured	*c* (kPa)	*φ* (º)
NA	yes	370.68	45.1
	no	257.67	43.6
CDA	yes	388.71	43.5
	no	219.25	42.1

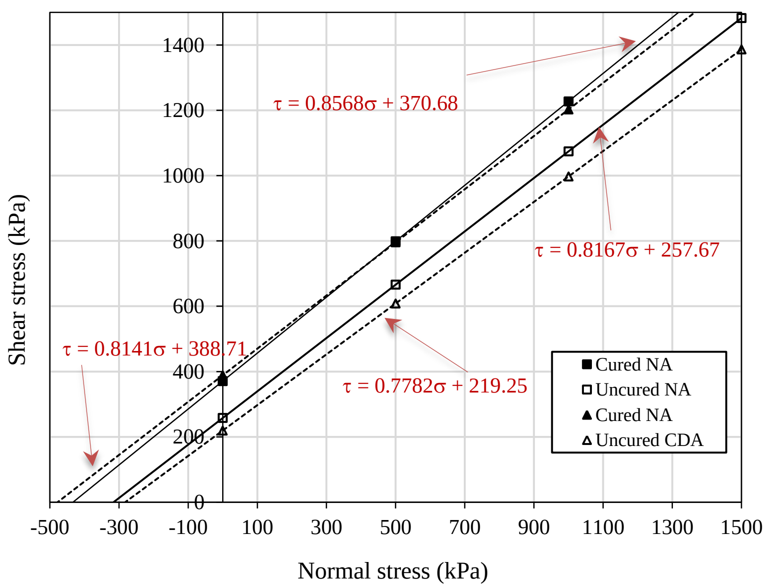

Fig. 3. Mohr–Coulomb envelopes obtained for BSM mixtures.

In Fig. 3, the Mohr–Coulomb envelopes are plotted using the values of the shear parameters of Table 3. As seen for the uncured samples, *c* was lower for the BSM with CDA that with NA. However, after curing, the *c* value of BSM with CDA increased and reached and even surpassed that of the BSM with

NA. The angle φ was greater for BSM with NA both before and after curing. However, all of the recorded values were similar and between 42º and 45º. In Fig. 3, the curves of both materials were very similar after curing. Therefore, after curing, BSM with an NA or a CDA will have very similar shear strength.

Cumulative axial permanent-strain model

The permanent deformation behaviour was determined by dynamic-load triaxial tests with CCP in accordance with Standard EN 13286-7 recommendations as published in Gómez-Meijide and Pérez [14]. The permanent deformation of the BSM base course was studied using a double exponential model that predicted the three phases of the cumulative axial permanent strain (ε_p) versus the number of load cycles (N) [10, 14] as

$$\varepsilon_p = A\left(\frac{N}{1000}\right)^B + C\left(e^{D\frac{N}{1000}} - 1\right), \qquad (4)$$

$$A = a_1(SR)^{a_2}; B = b_1(SR)^{b_2}; C = c_1(SR)^{c_2}; D = d_1(SR)^{d_2},$$

where a_1, a_2, b_1, b_2, c_1, c_2, d_1, and d_2 are fitted experimental coefficients. The values of the eight fitted coefficients for BSM materials with CDA and NA are listed in Table 4.

Table 4. ε_p model coefficients [14]

Aggregate	Cured	a_1	a_2	b_1	b_2	c_1	c_2	d_1	d_2
NA	yes	1.2902	0.692	0.00007	2.0299	$7\cdot10^{-13}$	5.7974	$1\cdot10^{-27}$	15.854
	no	0.4606	0.9308	0.00001	2.4538	$1\cdot10^{-35}$	19.303	$1\cdot10^{-36}$	20.649
CDA	yes	0.8552	0.7533	0.00005	2.0674	$5\cdot10^{-19}$	9.4728	$2\cdot10^{-19}$	10.784
	no	0.4261	0.8936	0.000001	2.7873	$1\cdot10^{-21}$	9.7506	$9\cdot10^{-46}$	24.703

The shear parameters were used to calculate the stress ratio (SR) expressed as the ratio between the acting deviator stress (σ_d) and the deviator stress at failure ($\sigma_{d,f}$) for the Mohr–Coulomb criterion [9]:

$$SR = \frac{\sigma_d}{\sigma_{d,f}} = \frac{\sigma_1 - \sigma_3}{\sigma_3\left[tan^2\left(45^0 + \frac{\varphi}{2}\right) - 1\right] + 2\,c\,tan\left(45^0 + \frac{\varphi}{2}\right)} \quad , \qquad (5)$$

where σ_1 and σ_3 are the major and minor principal stresses, and *c* and φ are the shear parameters listed in Table 3. Jenkins et al. [9] reported that SR is a critical parameter that expresses the mechanical response of BSM materials to permanent deformation. As the value of the SR increases, the ε_p value increases as well. According to Jenkins et al. [9], when the SR value is over 0.40, rutting may occur. It is important to find the critical position of the SR in the base course. To do this, σ_1 and σ_3 must be obtained using FLAC3D at different locations in the BSM base course which permit the computation of the SR by means of Equation 5. The critical position is the point with the maximum SR.

3.2. HMA wearing course

A linear elastic behaviour was assumed for the HMA wearing course: elastic modulus E = 5.0 x 10^6 kPa and ν = 0.35. A specific weight γ_{sat} = 24.0 kN/m^3 and a coefficient of earth pressure at rest of K_0 = 0.6 were assumed.

3.3. Cement-stabilised soil material

A linear elastic behaviour was considered for the 'in place' cement-stabilised fine-grained soil (CSS) subgrade with an elastic modulus E = 1.0 x 10^6 kPa and Poisson coefficient ν = 0.25. A specific weight γ_{sat} = 22.0 kN/m^3 and a coefficient of earth pressure at rest of K_0 = 0.6 were assumed.

3.4. Fine-grained soil

A nonlinear elastic model was adopted for the fine-grained soil subgrade [15, 23]:

$$M_r = k_1 + k_3(k_2 - \sigma_d) \qquad \sigma_d \le k_2,$$

$$M_r = k_1 + k_4(\sigma_d - k_2) \qquad \sigma_d \ge k_2, \tag{6}$$

where k_1 = 8.5·10^4 kPa, k_2 = 42.8 kPa, k_3 = 1,110 kPa, and k_4 = 178 kPa are coefficients obtained from dynamic triaxial tests [15, 23]. A specific weight γ_{sat} = 20.0 kN/m^3, a coefficient of earth pressure at rest of K_0 = 0.6, and a Poisson coefficient of ν = 0.35 were assumed.

4. Pavement section and numerical model

The section selected for the analysis was defined by the ATEB [19] for low-volume roads with BSM base courses, specifically for the traffic category T4: annual average daily heavy traffic ($AADT_{HT}$) ≤49 heavy vehicles/day. The section consisted of a 50-mm-thick HMA wearing course overlying a BSM-type material 120-mm-thick base course placed over a subgrade composed of two layers: an 'in place' 300-mm-thick CSS and a fine-grained soil (Fig. 4).

The Spanish standard 130-kN single axle with two dual tyres (65 kN carried by each set of dual tyres) was adopted as the load configuration for the analysis. Two homogeneous circular loads p of 0.90 MPa were applied with a radius a of 107.2 mm, and the distance between the radial centres was 343 mm (Fig. 4).

A numerical model to obtain the stresses and deformations produced in the pavement by the application of a load configuration on its surface was developed with FLAC3D 3.10 [24]. FLAC3D is a 3D program that uses a specific scheme of finite differences which permits the simulation of the elastic–plastic behaviour of the materials used in the pavement layers. By means of FLAC3D, the materials are represented by polyhedric elements forming a 3D grid that fits the shape of the modelled object. Each element behaves according to an established law of stress—strain (linear or nonlinear) in response to the applied loads and the boundary conditions. The material may yield and be plastically deformed. Figure 5 shows the grid of finite difference elements and the coordinate system used in the pavement section for the dual tyres. The model contained 2,500 elements and 2,900 nodes. Given the conditions of symmetry entailed in the problem (in terms of geometry and loads), only half of the real problem was studied taking care to impose the appropriate boundary conditions in the symmetry plane.

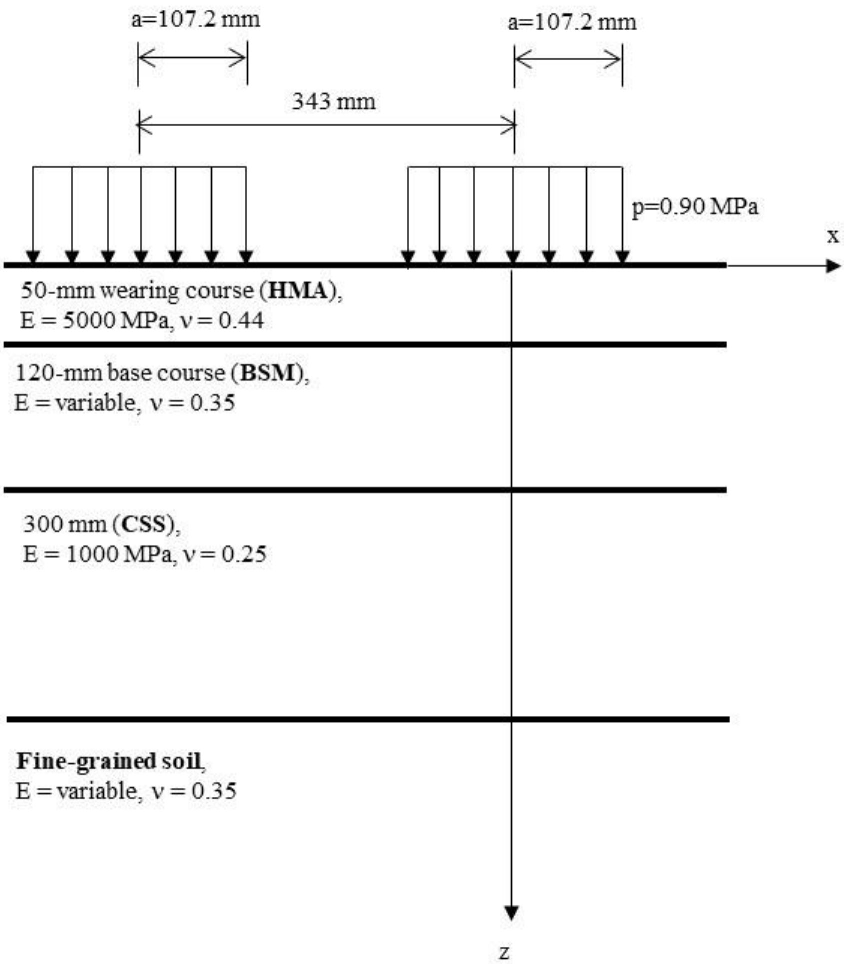

Fig. 4. Pavement section used for modelling.

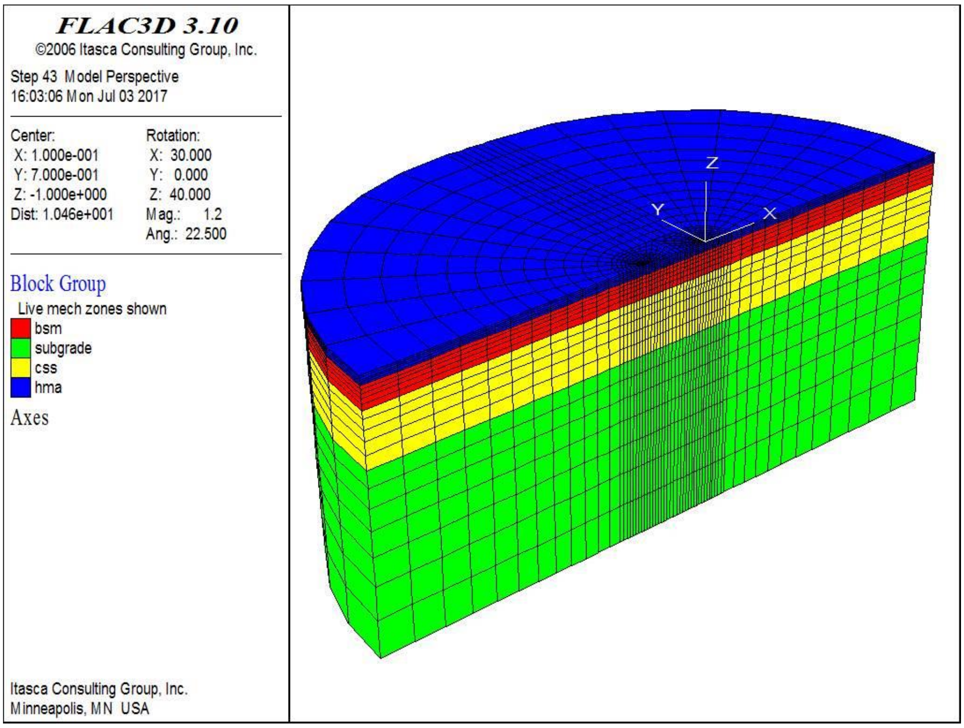

Fig. 5. Mesh and coordinate system.

The following boundary conditions were applied:

- Movement was banned in y-direction on plane y = 0 (symmetry plane).
- Movement was banned in the x- and y-directions on the lateral (circular) edge of the grid. The lateral edge of the grid was located 1.4 m from the dual tyres; therefore, it would have a minimal effect on the results.
- All movement was banned on the lower plane $z = -1.24$ m.
- The ground-water level was assumed to be very deep and therefore did not interfere with the numerical simulations as the materials were not submerged. Hence, the total stresses coincided with the effective stresses. The contact between the layers was one of total adherence (equality of horizontal deformations). The process reproduced with the numerical model consisted of two phases. The first phase provided the state of in-situ stresses existing in the pavement before applying the tyre loads. Once a state of mechanical equilibrium was reached for the specific weights and boundary conditions were applied, all model movements were reset to zero. In the second phase of the modelling, the tyre loads were applied.

5. Results and discussion

5.1. Predicted responses in BSM base course with three nonlinear models

The values of the three nonlinear models coefficients obtained experimentally (Table 2) were used in the FLAC3D model to obtain the variation of the M_r through the BSM base-course depth below the tyre loads (Fig. 6). In addition, three BSM base-course responses were monitored at the following critical points:

- Deflection in the BSM higher fibre (d_B) vs. distance to centre of dual tyres axle (Fig. 7).
- Tensile strain in BSM lower fibre (ε_{rB}) vs. distance to centre of dual tyres axle (Fig. 8).
- SR in the BSM higher fibre vs. distance to centre of dual tyres axle (Fig. 9).

5.1.1. Resilient modulus

The M_r variation through the BSM course depth predicted by the three models is shown in Fig. 6. The M_r was predicted for the BSM materials cured and uncured with NAs and CDAs. As can be seen in the four cases, as the depth of the BSM base course increased, the M_r diminished because the stresses diminished with the depth. Therefore, the BSM showed a clear nonlinear behaviour with stress dependency. The slopes of the curves predicted by the three models were similar. Equations 2 (Uzan model) and 3 (NCHRP model) predicted a similar M_r, and after 0.125-m depth, both equations practically predicted the same values. Furthermore, Equation 1 (Hicks model) predicted a higher M_r than Equations 2 and 3.

In the NA-BSM base course of the NCHRP model, after curing, the M_r varied between approximately 1.2 x 10^6 kPa and 1.5 x 10^6 kPa (Fig. 6a), and before curing, it fluctuated between 6.5 x 10^5 kPa and 8.0 x 10^5 kPa (Fig. 6b). The M_r of the CDA-BSM base course after curing varied between approximately 8.0 x 10^5 kPa and 1.1 x 10^6 kPa (Fig. 6c), and before curing it fluctuated between approximately 5.0 x 10^5 kPa and 6.5 x 10^5 kPa (Fig. 6d).

Therefore, as expected, the NA-BSM base course displayed a higher stiffness before and after curing than that of the CDA-BSM base course. Nevertheless, when the base courses were uncured, the stiffness difference between the BSM materials with NA and with CDA was less significant. Moreover, both the NA-BSM and CDA-BSM base courses displayed a higher stiffness after curing.

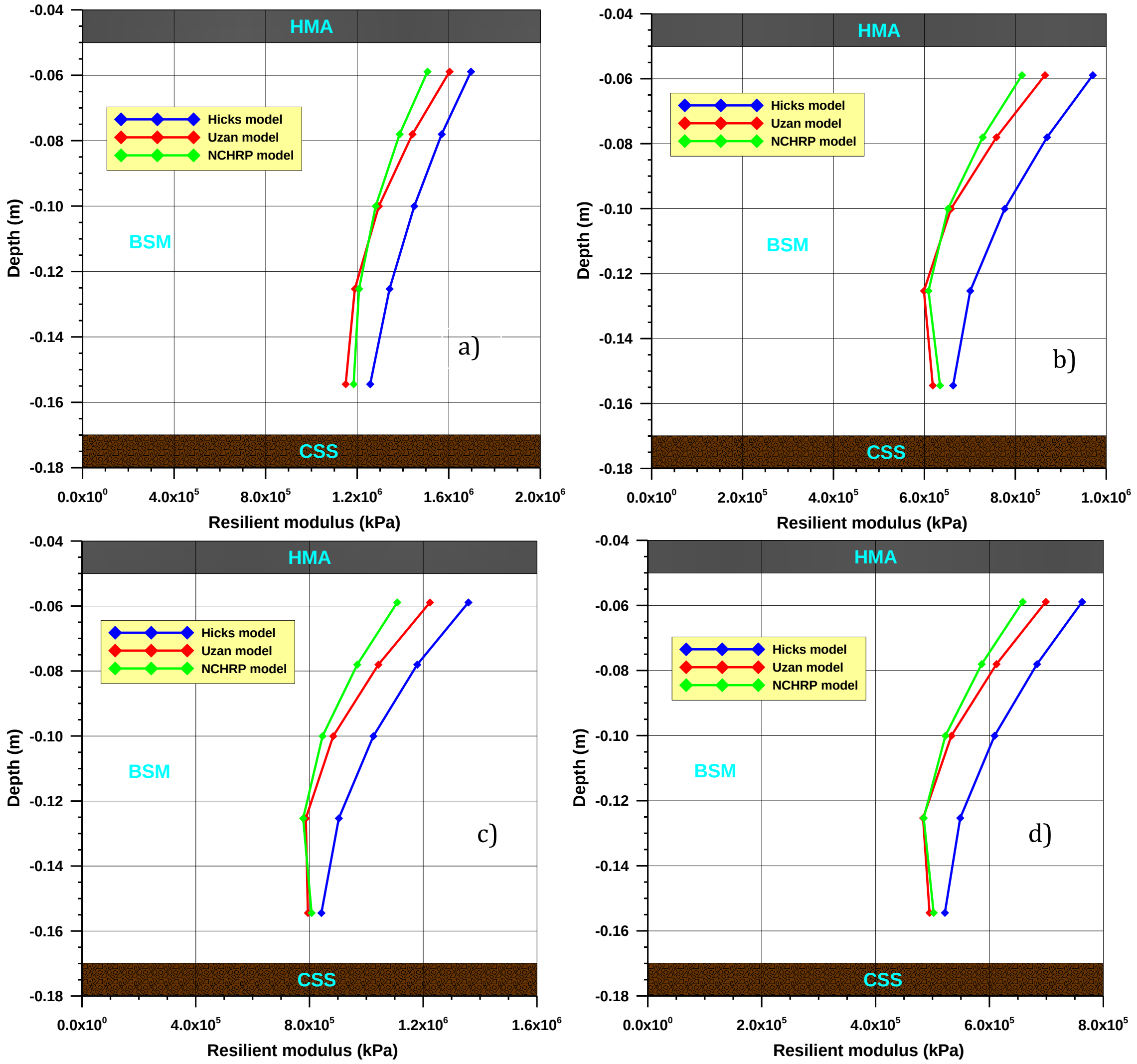

Fig. 6. Resilient modulus variation in BSM course: a) cured NA, b) uncured NA, c) cured CDA, and d) uncured CDA.

5.1.2. Deflections

The deflection variation in the BSM base-course higher fibre (d_B) for the three nonlinear models in the previous four conditions are shown in Fig. 7. The peak deflections were produced just below the two tyres, and the Uzan and NCHRP models predicted the same deflection values, while the Hicks model predicted slightly lower values (Table 5). This is expected because the Hicks model predicts a higher M_r (Fig. 6). Clearly, the cured BSM base courses had lower peak-deflection values, and the lowest deflections were produced in the NA-BSM.

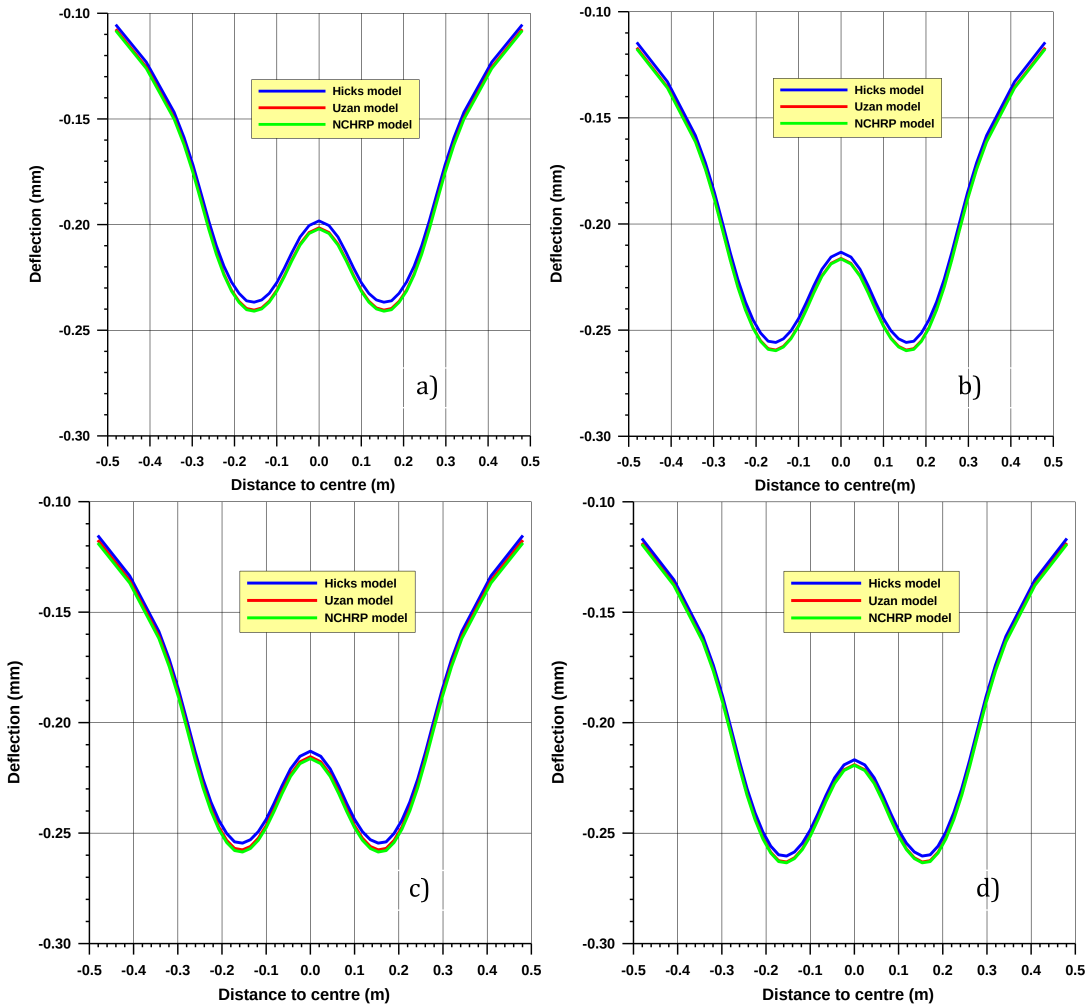

Fig. 7. Deflection variation of BSM base course of three models: a) cured NA, b) uncured NA, c) cured CDA, and uncured CDA.

5.1.3. Tensile strains

The tensile strains in the BSM base-course lower fibre (ε_{rB}) predicted by the three nonlinear models versus the distance to the axle-dual tyres centre are shown in Fig. 8. The peak tensile strains were produced just below the tyres. Moreover, the values of the tensile strains were at compression (minus sign) between approximately 0 m and 0.1 m and between 0.3 m and 0.9 m from the axe-dual tyres centre. The tensile strains were at traction (plus sign) below the tyres between 0.1 m and 0.3 m and beyond 0.9 m from the axe-dual tyres centre. The Uzan and NCHRP models predicted similar peak tensile strain values, while the Hicks model predicted slightly higher values (Table 5) as shown in Fig. 8. This was expected because the Hicks model predicts higher M_r values. The peak tensile strains were higher with cured NA-BSM base courses.

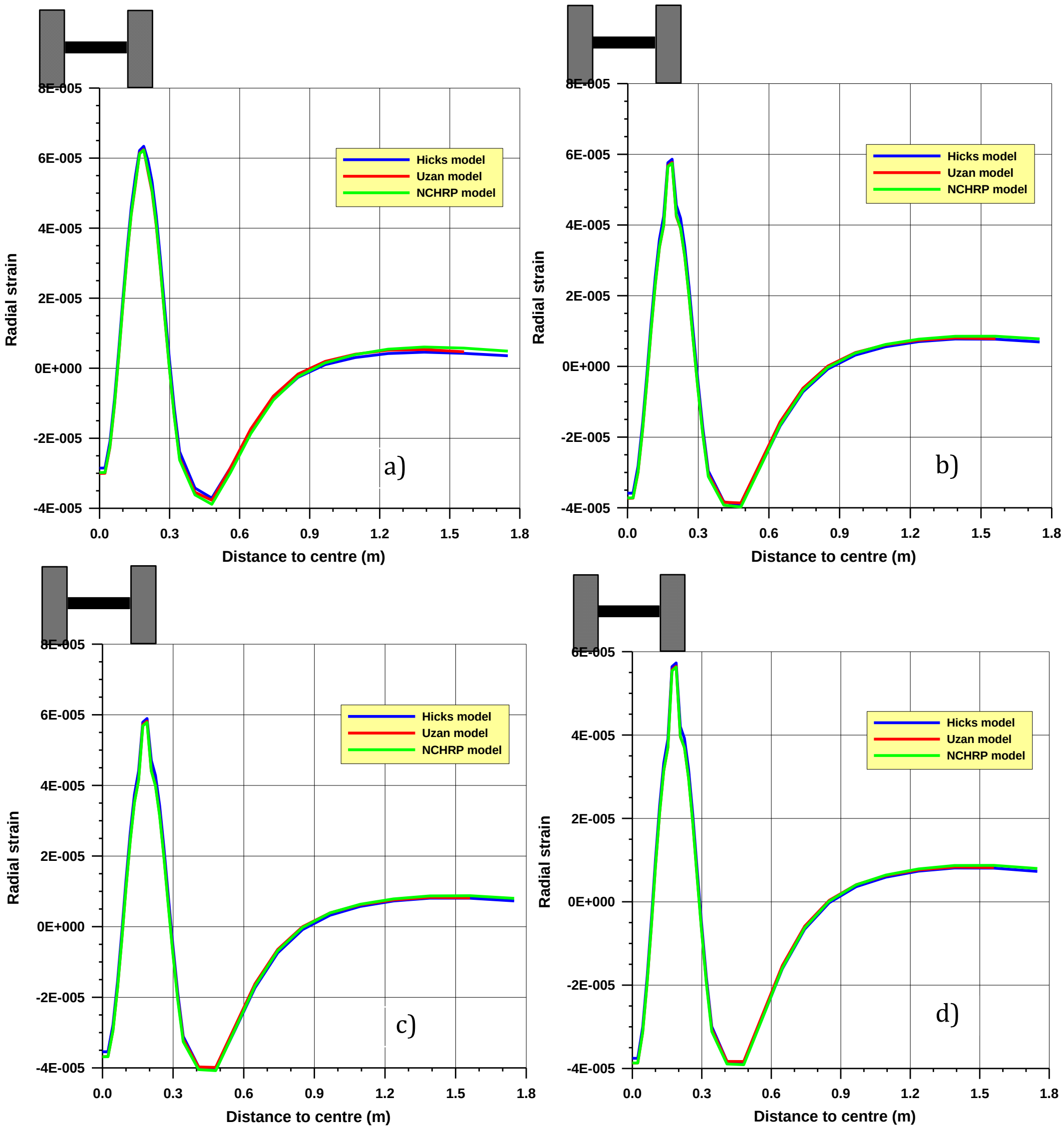

Fig. 8. Tensile strain variation of BSM base course of three models: a) cured NA, b) uncured NA, c) cured CDA, and d) uncured CDA.

Table 5. Peak predicted responses in BSM layer using three nonlinear models

Aggregate	Cured	Model: Hicks			Model: Uzan			Model: NCHRP		
		d_B (mm)	ε_{rB} ($\mu\varepsilon$)	SR	d_B (mm)	ε_{rB} ($\mu\varepsilon$)	SR	d_B (mm)	ε_{rB} ($\mu\varepsilon$)	SR
NA	yes	0.237	64.2	0.250	0.241	62.2	0.252	0.241	62.3	0.253
	no	0.256	58.9	0.362	0.260	58.1	0.360	0.260	57.4	0.362
CDA	yes	0.256	58.6	0.255	0.259	57.6	0.255	0.259	57.8	0.256
	no	0.261	57.5	0.435	0.264	56.3	0.432	0.264	56.3	0.434

5.1.4. Strain ratios

Figure 9 represents the SR calculated in the higher fibre of the BSM base course where the highest values were obtained versus the distance to the axle-dual tyres centre. The highest peak SR prediction values were produced at 0.25 m from the axle-dual tyres centre. Moreover, the three nonlinear models practically predicted the same highest peak SR (Fig. 9, Table 5).

Before curing, the peak SRs of the CDA-BSM were higher than those of the NA-BSM (Table 5). However, when the BSM was fully cured, the values of the peak SRs were similar in both types of aggregate. The curing of BSM materials produced a sharp decrease in the peak SR values, and this drop was even greater in the CDA-BSM base course.

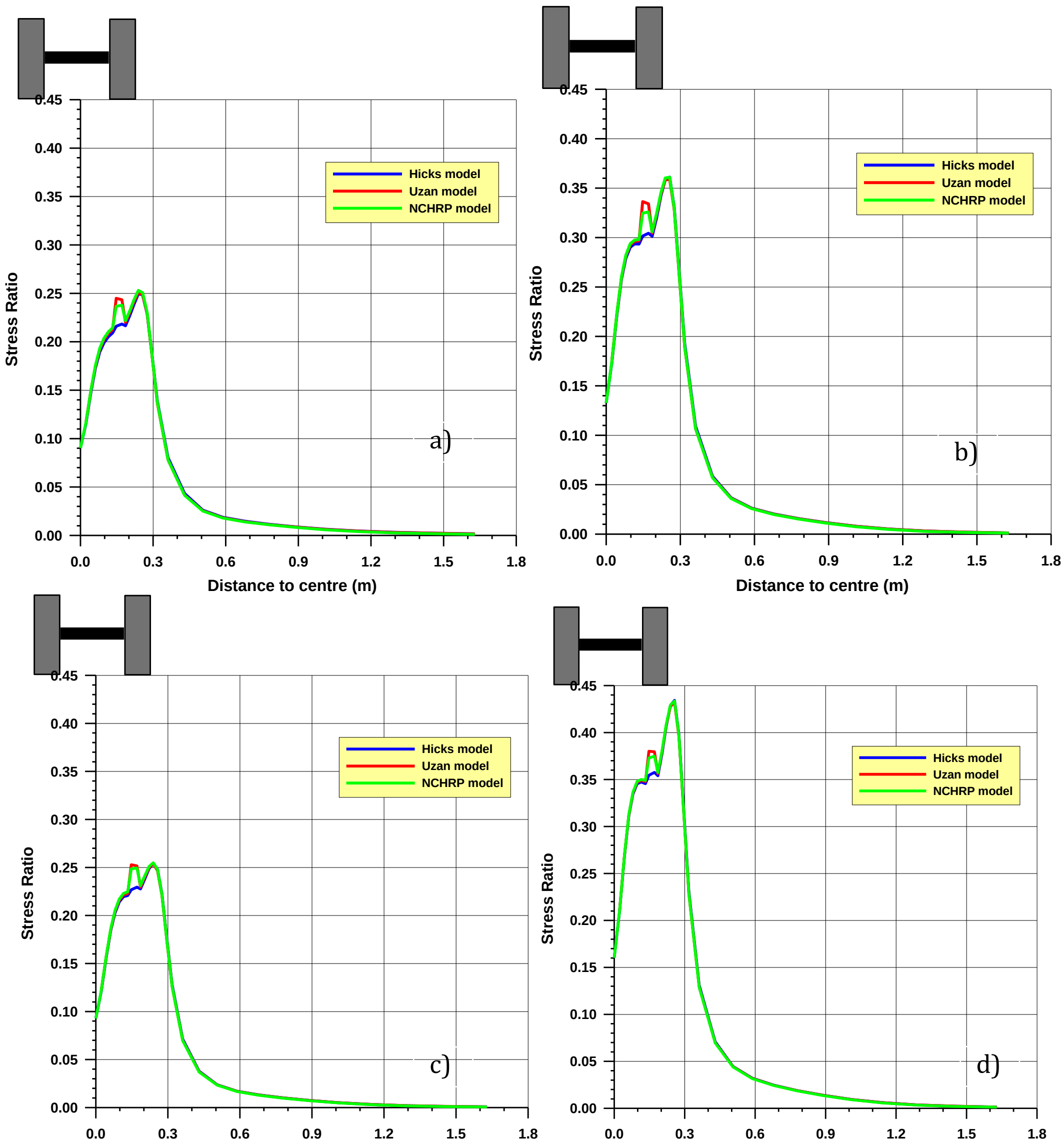

Fig. 9. SR variation on BSM base course of three models: a) cured NA, b) uncured NA, c) cured CDA, and d) uncurred CDA.

The peak SR predictions of the CDA-BSM base course before curing varied between 0.432 and 0.435 (Table 5). These values were higher than the 0.40 considered by Jenkins et al. [9] as the limit to prevent rutting in a base course. Therefore, if this limit is correct, rutting will occur in an uncured CDA-BSM base course. Finally, the three nonlinear models predicted similar deflections, tensile strains and SRs. The Hicks model was very easy to use and had a lower computational cost than the other models. Nevertheless, it predicted values slightly on the unsafe side because it predicted lower deflections. The Uzan and NCHRP model predictions were more similar. Nevertheless, the NCHRP model was the most modern and developed model and was selected for this study because of these considerations.

5.2. Stresses in pavement section

Having selected the NCHRP model, the vertical and horizontal stresses in the pavement were calculated. As shown in Fig. 10, the vertical stresses in the pavement were always in compression (negative sign) except in some HMA surface zones between the dual tyres and a distance from the tyres centre that were working at traction (positive sign). These compression stresses decreased with an increase in the pavement depth and with an increase in the radial distance to the centre of the tyres. In Fig. 10, the difference between the vertical stress values in the NA-BSM bases course and those in the CDA-BSM bases course were insignificant. Below the tyre load of the HMA lower fibre, the compression vertical stresses were between 700 kPa and 800 kPa, in the BSM lower fibre between 300 kPa and 400 kPa, and in the CSS lower fibre between 0 kPa and 100 kPa. At some points far from the load centre, the vertical stresses were working at a maximum value of 27.25 kPa.

The pavement horizontal stresses are shown in Fig. 11. In the HMA and CSS lower-fibre cases, the horizontal stresses were at traction, and the CSS-layer higher slice was at compression. Nevertheless, in the BSM base courses, the horizontal stresses were at compression, while as shown in Fig. 8, the tensile strains were at traction in the lower fibre. This occurred because the tensile strains shown in Fig. 8 were the result of only the tyre loads, while in the Fig. 11 the horizontal stresses (at the same lower fibres) were the result of not only the tyre loads but also the in-situ compressive stresses owing to the pavement's own weight.

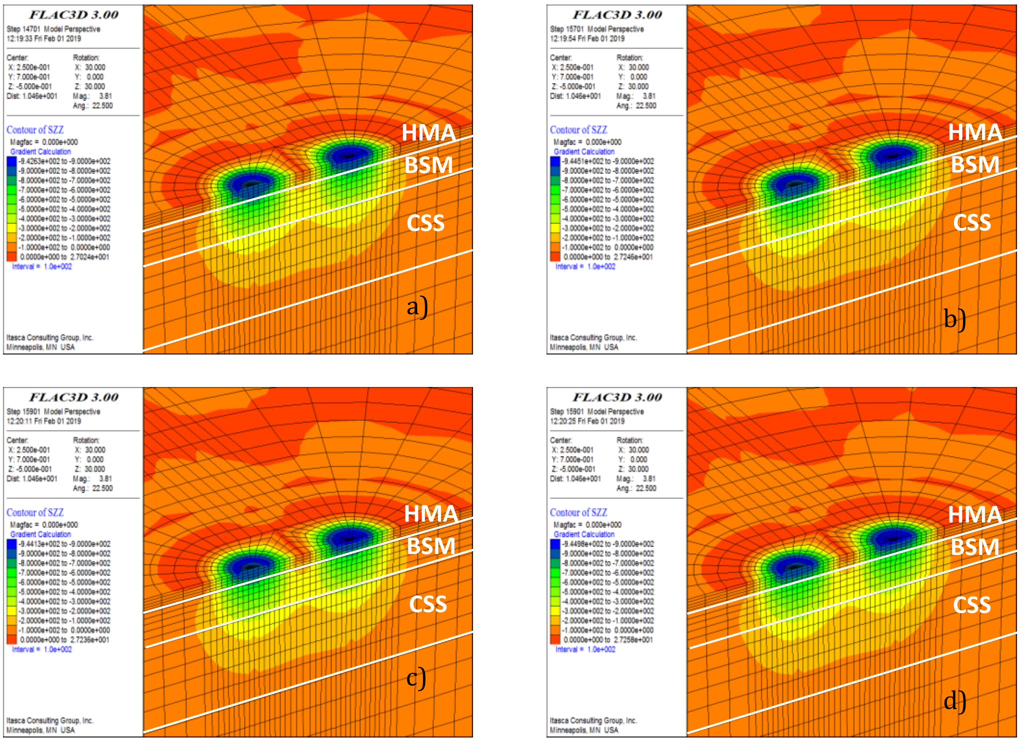

Fig. 10. Vertical stresses in pavement (negative sign indicates compression): a) cured NA, b) uncured NA, c) cured CDA, and d) uncured CDA.

Below the tyre loads, in the HMA and CSS-layer lower fibres, the traction horizontal stress values ranged between 0 kPa and 99.57 kPa (cured NA-BSM), 0 kPa and 124.16 kPa (uncured NA-BSM), 0 kPa and 94.43 kPa (cured CDA-BSM), and 0 kPa and 164.59 kPa (uncured CDA-BSM). Therefore, as in the HMA and CSS layers, the horizontal stresses at traction were similar when the CDA-BSM and NA-BSM base courses were cured. When the base courses were uncured, the horizontal stresses were higher in the CDA-BSM base course. In addition, the horizontal stresses at traction were higher before curing. The horizontal stresses of the BSM base courses were always at compression and between 0 kPa and 400 kPa for the two aggregates before and after curing.

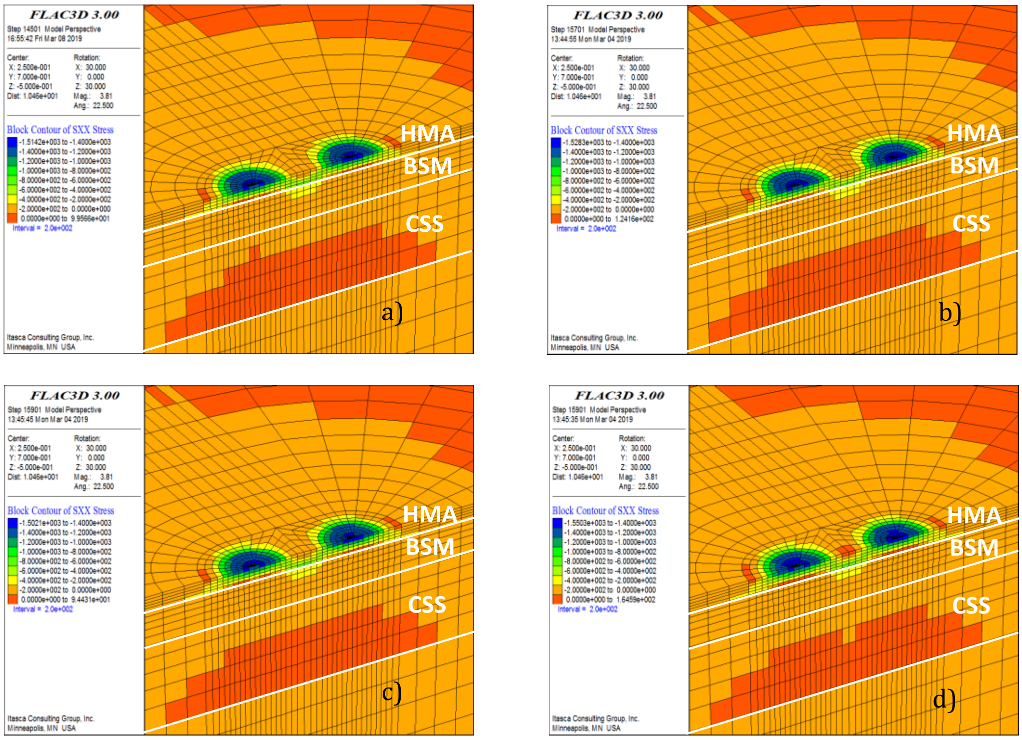

Fig. 11. Horizontal stresses in pavement (negative sign indicates compression): a) cured NA, b) uncured NA, c) cured CDA, and d) uncured CDA.

5.3. Peak responses in pavement layers of different thicknesses

The pavement critical peak responses were calculated by FLAC3D for several thicknesses of HMA wearing course and BSM base course. The thickness of the CSS layer was maintained at 300 mm. An analysis was performed to determine the effect of variations in the thickness of BSM base course and HMA wearing course on the performance of structural pavement layers. Seven pavement peak responses were analysed at the following critical points:

- HMA wearing course: peak vertical deflection on the surface (d_H) and peak tensile strain in the lower fibre (ε_{rH}) (Fig. 12),
- BSM base course: peak vertical deflection in the higher fibre (d_B), peak tensile strain in the lower fibre (ε_{rB}), and peak SR in the higher fibre (Fig. 13),
- CSS subgrade layer: peak tensile stress in the lower fibre (σ_r) (Fig. 14), and
- fine-grained soil subgrade: peak axial strain on the upper fibre (ε_v) (Fig. 15).

Each of the above-mentioned figures contain a legend. Using Fig. 12 as an example, the first term of the legend denotes the type of aggregate used in the BSM base course (NA or CDA), and the second term denotes the type of layer thickness variation (HMA wearing course or BSM base course). Thus, CDA-HMA means that the BMS base course is constructed with CDAs and the HMA peak responses are a function of the HMA thickness variation. NA-BSM means that the BMS base course was constructed with NAs and the HMA peak responses are a function of the BSM thickness variation. The x-axis represents the critical peak responses, the left y-axis (HMA thickness) varies between 3 cm and 10 cm, and the right y-axis (BSM thickness) fluctuates between 8 cm and 22 cm. Moreover, the peak response curves versus the HMA wearing-course thickness were made with a constant 12-cm BSM base course; while the peak response curves versus the BSM base course thickness were made with a constant 5-cm HMA wearing course. Therefore, the curves for the 5-cm wearing-course and the 12-cm BSM base-course thicknesses intercepted.

5.3.1. HMA wearing course peak responses

Peak deflections (d_H)

The variation of the HMA wearing-course peak responses when the BSM was cured is shown in Figs. 12a and 12c and when uncured in Figs. 12b and 12d. As shown in Figs. 12a and 12b, the HMA wearing-course peak deflections increased with a constant 12-cm BSM base-course thickness and a decrease in the HMA wearing-course thickness from 10 cm to 3 cm. The peak deflections were higher when the BSM base course was made with CDA because of its lesser stiffness. Moreover, when the two BSM base courses were cured, the difference between the two peak deflection curves was higher (Fig. 12a). Thus, after curing, the difference between the two curves was approximately 2×10^{-2} mm and before curing was only approximately 5×10^{-3} mm. These occurrences resulted because the two uncured BSM materials had a similar M_r, while the cured BSM base courses with NA and CDA had very different values of M_r (Fig. 6).

However, with a constant 5-cm HMA wearing-course thickness and a decrease of the BSM base-course thickness from 22 to 8 cm, the HMA wearing-course peak deflections only increased slightly when the cured BSM base course was made with NA (Fig. 12a). When the cured BSM was made with CDA, the deflections were constant (Fig. 12a), and the peak deflections practically had constant values for different BSM base-course thicknesses when the two uncured BSM base courses were made with

NA and CDA (Fig. 12b). The variation of the BSM base-course thickness had practically no effect on the HMA wearing-course peak deflections because the CCS subbase stiffness was similar or even higher than that of the BSM base-course (Fig. 6).

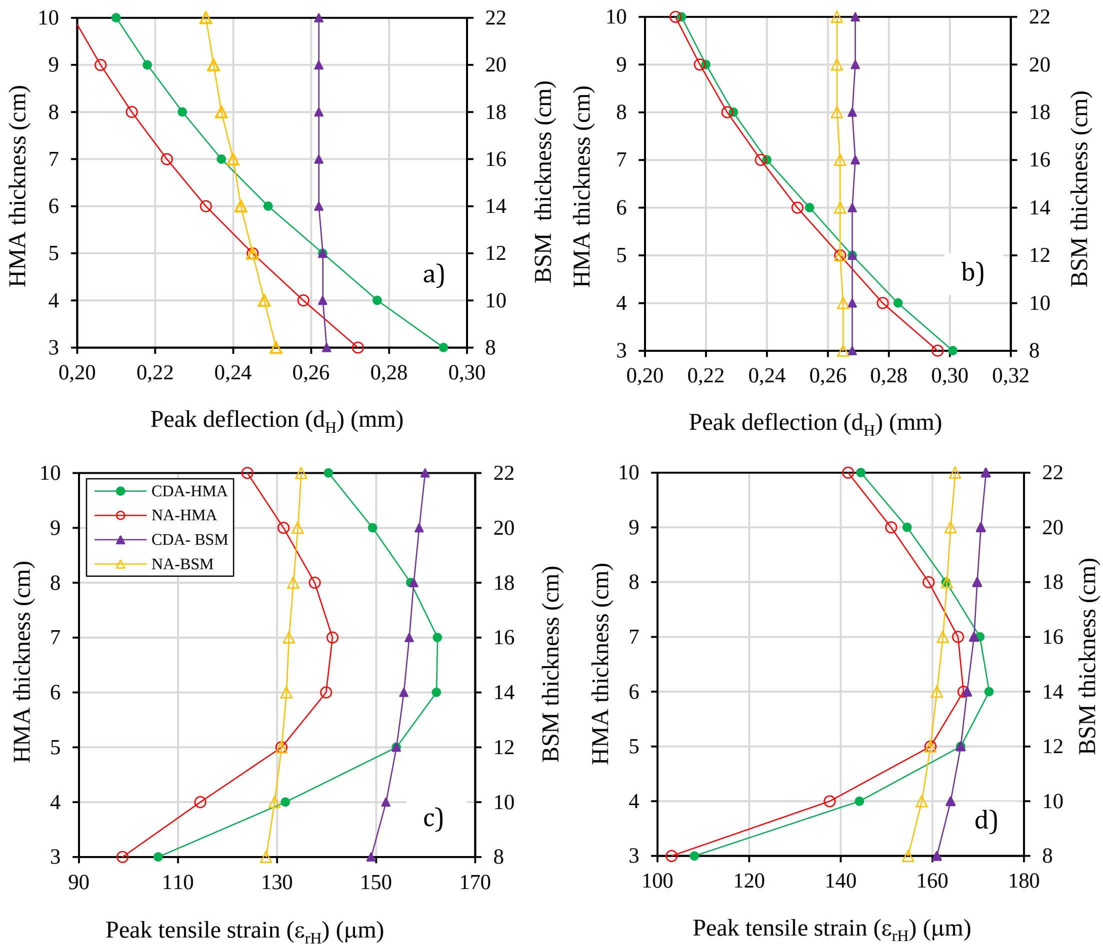

Fig. 12. Peak responses in HMA wearing course: a) peak deflection, cured BSM, b) peak deflection, uncured BSM, c) peak tensile strain, cured BSM, and d) peak tensile strain, uncured BSM.

Once more, when the BSM base courses were uncured, the peak deflections were higher with CDA. In addition, the differences between the peak deflections were approximately 15–29 x 10^{-3} mm higher after the BSM curing with CDA. Before the curing, the differences were only 3-6 x 10^{-3} mm.

Peak tensile strain (ε_{rH})

As shown in Figs. 12c and 12d, the HMA peak tensile strains were higher when the BSM base courses were uncured. Moreover, before and after curing, the peak tensile strains in the HMA lower fibre were higher when CDAs were used because the BSM base course with CDAs was less stiff and therefore absorbed less tensile strains. Consequently, the peak tensile strains in the HMA were higher. However, the curing of the two types of BSM base courses made with NAs and CDAs decreased the peak tensile strain values. This decrease occurred because a cured BSM base course is stiffer and therefore absorbs more tensile strains; consequently, the peak tensile strains in the HMA were lower. Also, the difference between the values of the peak tensile strain curves of the two BSM materials were higher after curing.

As shown in Figs. 12c and 12d, the peak tensile strain curves had a maximum value with a constant 12-cm BSM base-course thickness and a variation of the HMA wearing-course thickness from 3 cm to 10 cm. In other words, there was a critical thickness. Below the critical thickness, the tensile strain increased with a decrease in the HMA thickness, whereas above the critical thickness, the tensile strain decreased with a decrease in the HMA thickness. This performance was observed previously in flexible pavements constructed with bituminous wearing courses upon unbound granular materials [15]. The explanation is that, above the critical thickness, the wearing course provides an '*elastic structural layer action*', whereas below a thinner layer exhibits a '*membrane type behaviour*' [23]. In addition, after curing, the two maximum peak tensile strains were achieved for a 7-cm HMA wearing course and a 12-cm BSM base course with peak values of 141 με in the NA-HMA curve and 162 με in the CDA-HMA curve, respectively. Before curing, two maximum peak tensile strains were achieved for a 6-cm HMA wearing course and 12-cm BSM base course at 163 με in the NA-HMA curve and 173 με in the CDA-HMA curve, respectively.

As shown in Figs. 12c and 12d, the peak tensile strains in the HMA lower fibre decreased slightly with a constant 5-cm HMA wearing course thickness and a variation of the BSM base course thickness from 22 cm to 8 cm. Again, the peak tensile strain curve differences were higher after curing. Note that the variation of the BSM base-course thickness did not have a significant effect on the HMA wearing-course peak tensile strains. Even so, there was a small decrease in the peak tensile strains with a decrease in the BSM base-course thickness.

5.3.2. BSM base-course peak responses

Peak deflections (d_B)

Figs. 13a and 13b show the variation of the BSM base-course peak vertical deflections when the BSM is cured and uncured. The effect of a decrease in the HMA wearing-course thickness is more significant than that of a decrease in the BSM base-course thickness. The curves in Figs. 13a and 13b corresponding to the BSM base-course peak deflection values were very similar to those of the HMA wearing-course peak deflection (Figs. 12a and 12b). Therefore, the former explanations of section 5.31.1 are valid for Figs. 13a and 13b. The peak deflections of the BSM base courses were lower than those of the HMA wearing courses despite an approximate difference of 4 x 10^{-3} mm. Figs. 13a and 13b show that the intercept values were the same as the predicted values in Table 5 (HMA thickness of 5 cm and BSM thickness of 12 cm).

Peak tensile strain (ε_{rB})

Figs. 13c and 13d represent the variation of the BSM base-course peak tensile strains. The peak tensile strains increased with a decrease in the HMA wearing course and the BSM base-course thicknesses. In this case, the peak tensile strains were higher when the BSM base courses were made with NAs and after curing. After curing, the difference between the HMA wearing-course curves was approximately 4 $\mu\varepsilon$, and the BSM base-course curve differences were between 8.5 and 4.4 $\mu\varepsilon$. Before curing, the difference between the HMA wearing-course curves was approximately 1 $\mu\varepsilon$, and the BSM base-course curve differences were between 2.6 and 1 $\mu\varepsilon$.

As previously mentioned, when the BSM base courses were cured, the stiffness was higher and the tensile strains increased. However, the peak tensile strains were lower in the BSM base courses made with CDA because their stiffnesses were lower. Comparing Figs. 13c and 13d to Figs. 12c and 12d, the HMA wearing-course peak tensile strain values were in the order of two to three times higher. Therefore, fatigue problems are not expected in the BSM base courses.

Peak strain ratios

Figs. 13e and 13f show the variations of the peak SR values in the BSM base course. The decrease in the BSM base-course thickness had practically no influence on the peak SR values because the CSS-layer stiffness was similar or even higher than that of the BSM base-course stiffness. Nevertheless, a decrease in the HMA wearing-course thickness had an influence on the peak SR values because it increased the peak SR values.

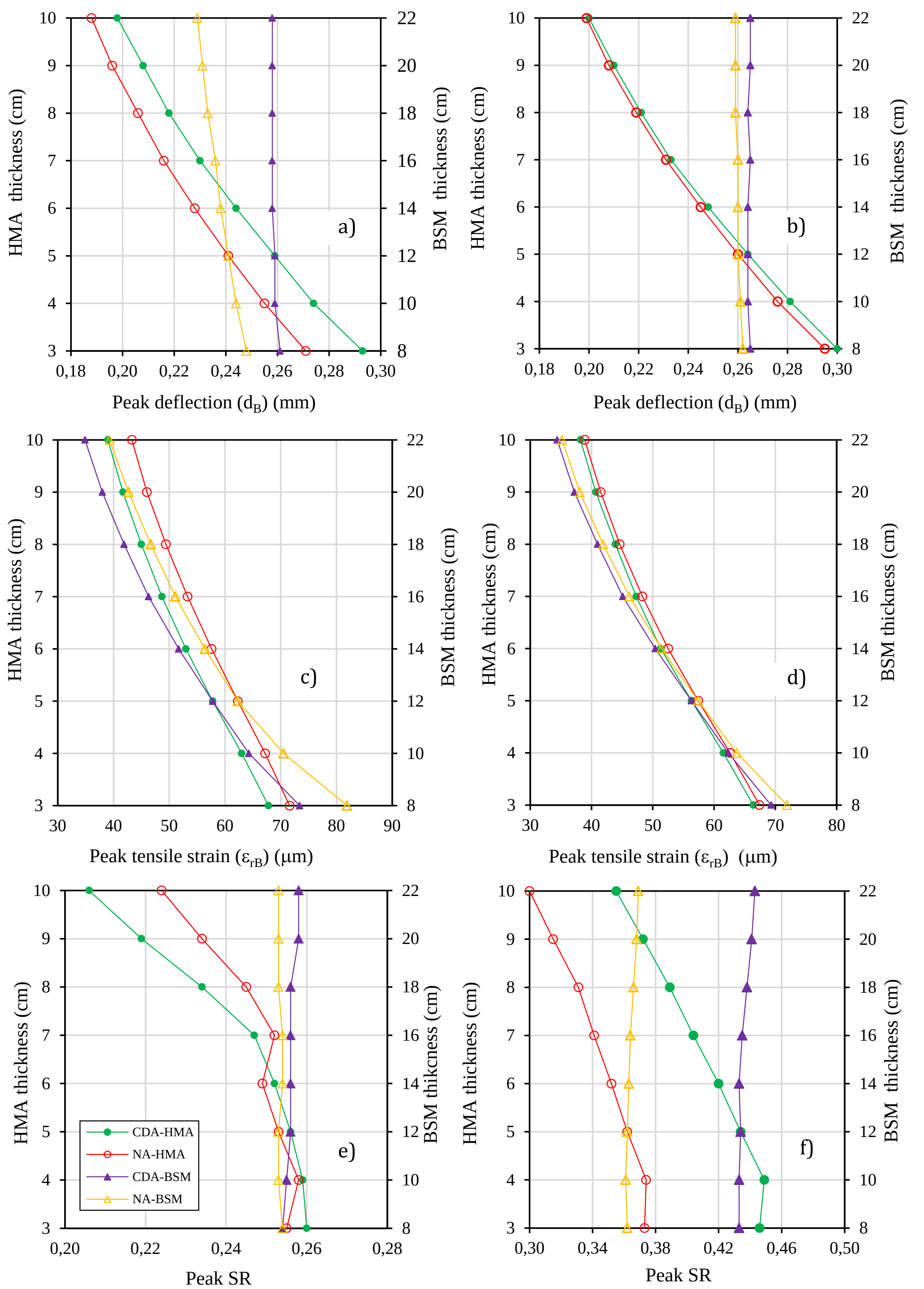

Fig. 13. Peak responses of BSM base course: a) peak deflection, cured BSM, b) peak deflection, uncured BSM, c) peak tensile strain, cured BSM, d) peak tensile strain, uncured BSM, e) peak SR, cured BSM, and f) peak SR, uncured BSM.

As expected, before curing, the peak SR values were higher and generally higher when CDA was used. After curing, the difference between the BSM base-course curves was approximately 3 x 10^{-3}.

Before curing, the difference between the BSM base courses was approximately 7 x 10^{-2}.

5.3.3. CCS-layer peak tensile stress

Figs. 14a and 14b reflect the curves of the variation of the peak CSS tensile stress (σ_r) values. A decrease in the HMA wearing-course thickness increased the peak CSS tensile stress values. Also, a decrease in the BSM base-course thickness increased the peak CSS tensile stress values. The peak CSS tensile stress values were slightly higher before the BSM base course was cured. When NA aggregates were used in the BSM base course, the peak CSS tensile stress values were lower than those when CDA aggregates were used. The difference in the peak CSS tensile stresses when the BSM base course was made with NA and when the BSM base course was made with CDA was approximately 2 kPa after curing (Figure 14a) and 1 kPa before curing (Figure 14b).

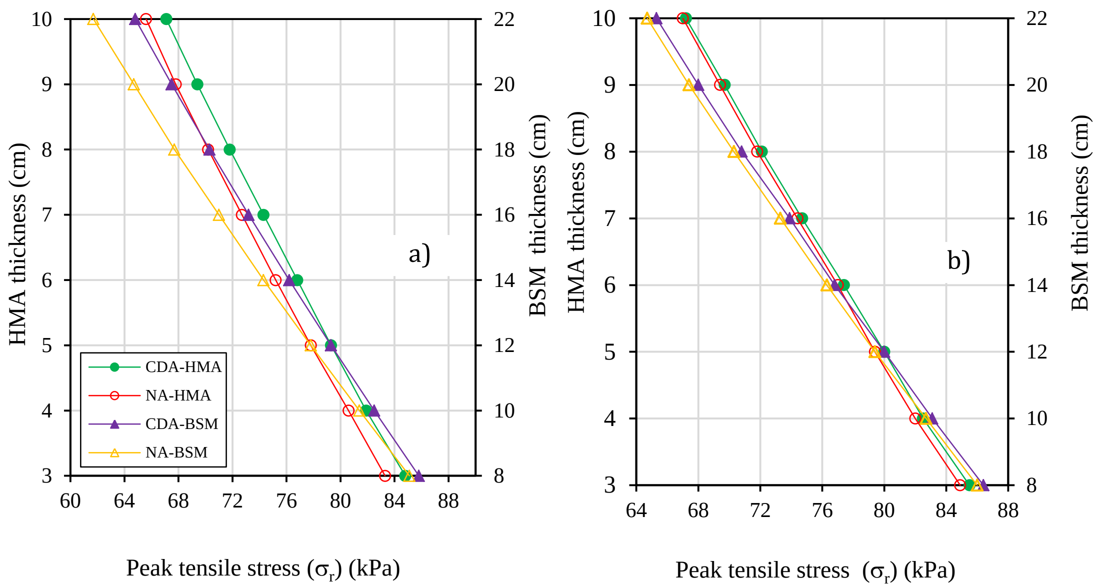

Fig. 14. Peak tensile stress in CCS layer: a) cured BSM and b) uncured BSM.

5.3.4. Fine-grained soil subgrade peak axial strain

Figs. 15a and 15b show the fine-grained soil peak axial strain (ε_v) variation curves. The peak ax ial strains always increased with a decrease in the HMA wearing-course and BSM base-course thicknesses. With CDAs, the peak axial strains were always higher, and the peak axial strains were lower after curing.

Finally, as presumed and explained in Section 5.3, a decrease in the BSM base-course thickness had no significant effect on either the peak deflection or the SR values of the HMA and BSM layers. Therefore, it is feasible to reduce the BSM base-course thickness. Nevertheless, a decrease could be counterproductive as it increases the HMA and BSM peak tensile strains. In addition, it increases the CCS-layer peak tensile stress and the fine-grained soil subgrade peak axial strain.

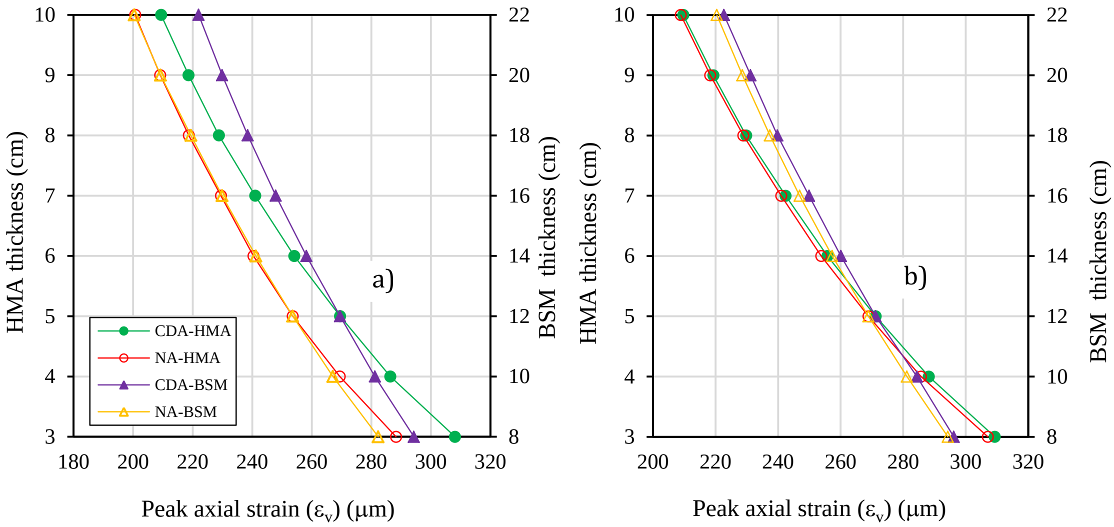

Fig. 15. Peak axial strain in fine-grained soil (S): a) cured BSM and b) uncured BSM.

5.4. BSM base-course axial cumulative permanent strain

The shear parameters of Table 3 (c and φ) were introduced into Equation 5 to calculate the maximum SR. Then, the parameters of Table 4 were used in Equation 4 to estimate the axial cumulative permanent strain (ε_p) in the BSM base courses. Fig. 16 shows the ε_p(%) versus the number of load cycles (N), where logically ε_p(%) increases with an increase in N. Figs. 16a and 16b show eight curves representing ε_p(%) versus N after and before curing, respectively. In each figure, four curves are BSM base courses made with NA, and four curves are made with CDA. In both figures, the curves with NA and CDA had a constant 12-cm BSM base-course thickness and four different HMA wearing-courses thickness of 3, 5, 7, and 9 cm.

As can be seen in Fig. 16a, when the BSM bases courses were cured, ε_p(%) increased with a decrease in the HMA wearing-course thickness. In this sense, ε_p(%) increased because the maximum SR increased as a result of a decrease in the HMA wearing-course thickness. Moreover, in the cured BSM base courses, the CDA ε_p(%) values were lower than those of the NA.

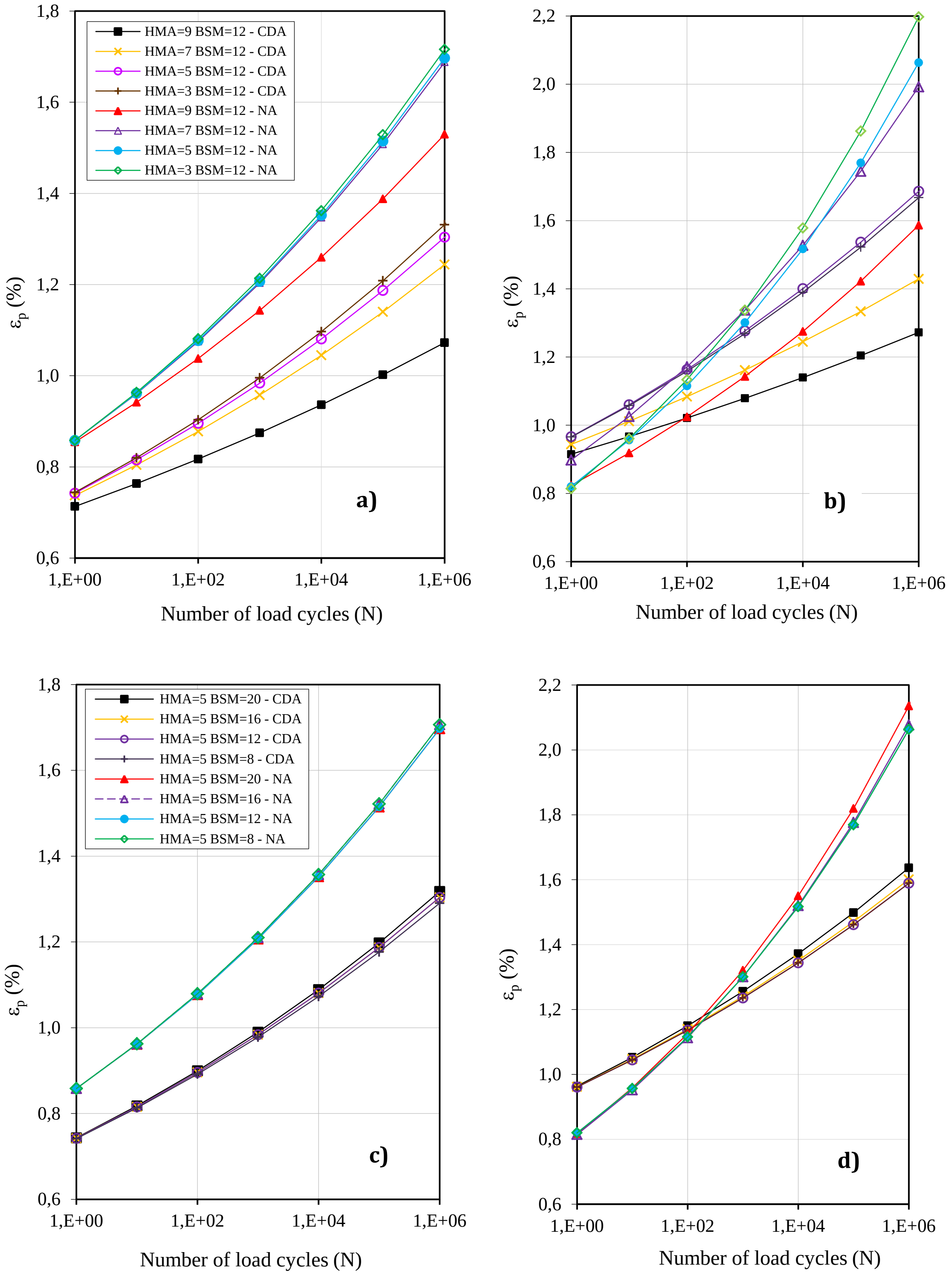

Fig. 16. BSM base courses ε_p versus number of load cycles: a) HMA variation, cured BSM, b) HMA variation, uncured BSM, c) BSM variation, cured BSM, and d) BSM variation, uncured BSM.

Therefore, when the material is cured, the BSM base courses made with CDA have higher resistance to permanent deformation. However, as shown in Fig. 16b, in the uncured BSM base courses, after approximately 1,000 N, the CDA ε_p(%) values were lower than those of the NA (except HMA = 9 and

BSM = 12 - NA). Before 1,000 N, it is unclear if the BSM base courses made with CDAs had a lower ε_p(%). In this case, the comparison between the two BSM materials must be made with a relatively low N because in a real case, the number of load cycles until the BSM base-course curing is not very high. Therefore, when the two materials (CDA or NA) are uncured, it is ill-defined which BSM base course has the higher resistance to permanent deformation.

Fig. 16c shows the eight curves of ε_p(%) versus N after curing, and Fig. 16d shows the eight curves of ε_p(%) versus N before curing at a constant 5-cm HMA wearing-course thickness and four BSM base courses with thicknesses of 8, 12, 16, and 20 cm. Fig. 16a shows the eight curves of ε_p(%) versus N after curing, and Fig. 16b shows the eight curves of ε_p(%) versus N before curing.

In Fig. 16a, clearly, when the base courses were cured, the CDA curves had a lower ε_p(%) than that of the NA curves. Nevertheless, in Fig. 16b, when the BSM base courses were uncured, the CDA curves had a lower ε_p(%) than that of the NA curves only after 100 load cycles. In this case, when the material was cured, the ε_p(%) curves were similar. Therefore, the BSM base-course thickness variation had an insignificant influence on the ε_p(%) values. Moreover, before the BSM material was cured as shown in Fig. 16b, the curves were very similar. Thus, the BSM base-course thickness influence was also insignificant.

As a final point of this section, it is necessary to clarify why in Figure 16 the BSM base courses made with CDA had less ε_p (%) than the BSM base courses made with NA. It is believed that when the BSM with CDA was subjected to a high number of triaxial load cycles a stiffening of the mortar rich in bitumen matrix produced the increase of the resistance to the permanent strain in the BSM with CDA. Therefore, when equation 4 was fitted to the cumulative axial permanent strain curves, the prediction of ε_p (%) in the BSM with CDAs was lower (Figure 16) and therefore there will also be lower rutting.

5.5. BSM base-course rutting during design period

As described in Section 4, the load configuration adopted was the standard 130-kN single axle with two dual tyres. Therefore, rutting was formed by single-axle loads of 130 kN with dual tyres upon the pavement section. Then, the rut depth (mm) formed in the BSM base course was estimated as the product of ε_p and the BSM base-course thickness in mm.

The pavement section was designed for a low-volume road with an AADT_{HT} of 49 heavy vehicles/day that was supported in the service lane during the project period. This heavy traffic flow was used to estimate the number of equivalent single-axle loads of 130 kN in the service lane during the design analysis period (N_T). For this purpose, the following equation was used [25]:

$$N_T = \mathrm{AADT}_{HT} \cdot \mathrm{C} \cdot \mathrm{A} \cdot 365 \cdot \gamma_T, \qquad (7)$$

where A is the heavy-vehicle equivalency factor of a single axle (0.70); γ_t is the safety coefficient related to the degree of uncertainty of measurement of heavy-load vehicles (1.15); C = $[(1+r)^n-1]/r$ is the traffic growth factor (24.30) with an annual growth rate, r, of 0.02; and n is the 20-year analysis period. Substituting these values into Equation 7, N_T = 3.4986 x 10^5 equivalent single-axle loads of 130 kN.

However, it is hypothesised in Spain that the real length of time for the in-situ curing of BSM base-course mixes is six months [19]. Therefore, in Equation 7, C = 0.5 years, and the number of equivalent single-axle loads of 130 kN during the curing period is N_{Tbc} = 7.1987 x 10^3. Accordingly, the number of equivalent single-axle loads of 130 kN during the design life period after curing is $N_{Tac} = N_T - N_{Tbc}$ = 3.4986 x 10^5 – 7.1987 x 10^3 = 3.4266 x 10^5 equivalent single-axe loads of 130 kN.

Table 6 lists the ε_p(%) and the rutting originated in pavement sections with different HMA wearing-course and the BSM base-course thicknesses. Some of these pavement sections were the same as those analysed in Fig. 16. Each pavement section ε_p(%) was obtained using Equations 4 and 5. The ε_p(%) and the rut depths produced during the design life period in the BSM base courses made with NAs and CDAs after curing were estimated using 3.4266 x 10^5 loads (Table 6). Thus, for the reference 120-mm BSM base-course thickness (Fig. 4) in the cured BSM base course made with NA, the estimated rut depth was 1.93 mm, and in the BSM base course made with CDA, the estimated rut depth was 1.50 mm. In addition, in Table 6 the ε_p(%) and the rut depths produced during the curing period in the BSM base courses made with NAs and CDAs were estimated using 7.1987 x 10^3 loads. Thus, for the reference 120-mm BSM base course thickness, during the curing period in the BSM made with NA, the estimated rut depth was 1.78 mm, and in the BSM made with CDA, the estimated rut depth was 1.60 mm. Obviously, the ε_p(%) predicted by equation 4 and the rut depth are lower during the design life after curing due to the increase in both the resilient modulus and shear strength parameters after the curing of the BSM base courses.

Table 6. Rutting in BSM base course

Thickness (mm)		Design life after curing (3.4266 x 10^5 load cycles)				Curing period (7.1987 x 10^3 load cycles)			
		NA		CDA		NA		CDA	
HMA	BSM	ε_p (%)	Rutting (mm)	ε_p (%)	Rutting (mm)	ε_p (%)	Rutting (mm)	ε_p (%)	Rutting (mm)
90	120	1.46	1.75	1.04	1.25	1.26	1.51	1.13	1.36
70		1.60	1.92	1.19	1.43	1.50	1.80	1.23	1.48
50		1.61	1.93	1.25	1.50	1.48	1.78	1.33	1.60
30		1.63	1.95	1.27	1.53	1.54	1.85	1.37	1.65
50	200	1.61	3.22	1.26	2.52	1.51	3.03	1.35	2.71
	160	1.62	2.59	1.25	2.00	1.49	2.38	1.33	2.14
	120	1.61	1.93	1.25	1.50	1.48	1.78	1.33	1.60
	80	1.62	1.29	1.24	0.99	1.48	1.19	1.33	1.06

Table 7. Total rutting during pavement design and pavement total rutting allocated to BSM base course

Thickness (mm)		Total rut depth in BSM during design life (mm)		% of 20-mm failure rut on surface assigned to BSM	BSM failure rut depth (mm)
HMA	BSM	NA	CDA		
90	120	3.27	2.61	53	10.60
70		3.72	2.91	55	11.00
50		3.71	3.10	57	11.40
30		3.80	3.18	59	11.80
50	200	6.25	5.23	65	13.00
	160	4.97	4.14	61	12.20
	120	3.71	3.10	57	11.40
	80	2.49	2.06	53	10.60

Moreover, in Table 6, in the constant 120-mm BSM base-course thickness, an increase in the HMA wearing-course thickness produced an ε_p(%) and decreased rutting. Nevertheless, with a constant 50-mm HMA thickness, an increase in the BMA base-course thickness produced similar ε_p(%) values, but the rutting values increase considerably.

In Table 6, the BSM base courses made with CDAs had less rutting that the BSM base courses made with NAs. In particular, in Table 6 when NAs were used, the rutting formed in the BSM base course during the curing period was lower than the rutting produced after curing. On the contrary, when CDAs were used, the rutting formed in the BSM base course during the curing period was higher than that after curing. Then, the rutting of both periods was summed to obtain the total rutting during the design life period in the reference base course was 3.71 mm when NA was used and 3.10 mm when CDA was used (Table 7). Note that 48% and 52% of the total rutting was reached only during the curing periods in the BSM base courses with NA and CDA, respectively (Table 7).

According to Liebenberg and Visser [26], in South Africa an appropriate rutting failure criterion for low-volume roads made with BSM base courses is a 20-mm rut depth on the pavement surface. Roos [27] performed a pavement analysis in South Africa to calibrate a new transfer function. In this analysis, the rut depth was measured in full pavement section structures at different times after construction, and the percentage of rutting attributed to BSM layers was estimated based on:

1. BSM thickness: the rutting percentage assigned to a BSM increase when the BSM thickness increased (Fig. 17a),
2. Asphalt layer thickness: the rutting percentage assigned to a BSM decrease when the HMA thickness increased (Fig. 17b), and
3. Type of supporting layer under the BSM: Weak support layers result in smaller percentages of rutting attributed to the BSM, while strong support layers result in higher percentages of rutting attributed to the BSM.

The adjustment factors used by Roos for the asphalt and BSM layers are shown in Fig. 17.

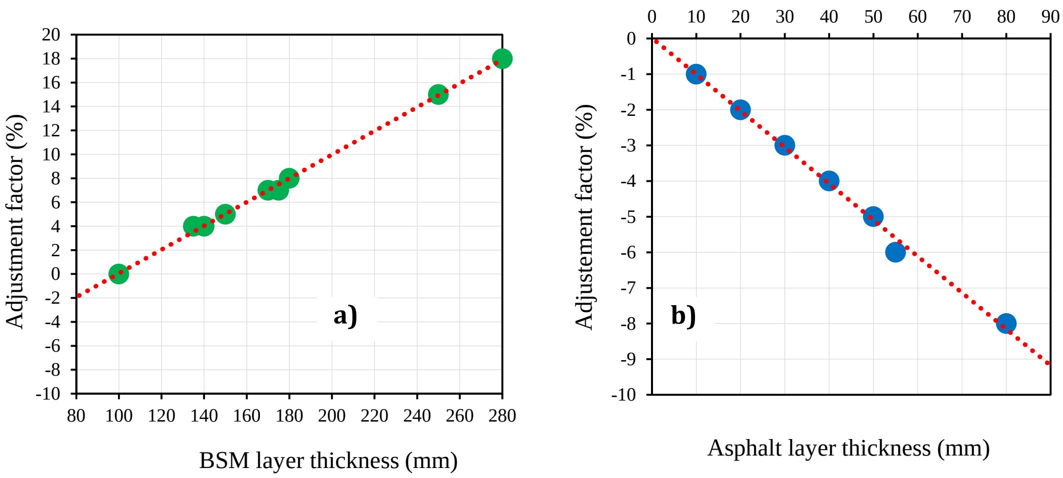

Fig. 17. Rutting adjustments: a) BSM layer thickness and b) asphalt layer thickness [27].

In the case of a strong support made with cement, the adjustment factor was 10%. Roos assigned an initial 50% of rutting to a 100-mm-thick BSM base course and adjusted this percentage according to the three former criterions. The adjustment factors shown in Fig. 17 were used to calculate the percentage of the failed 20-mm rut on the surface assigned to the BSM base course and to estimate the rut-depth failure (Table 7). For example, for a pavement section with a 50-mm HMA wearing course and a 120-mm BSM base course, the percentage of the 20-mm rut assigned to the BSM base course was 50 + 2 – 5 + 10 = 57%. Then, the 20-mm failed rut depth in the BSM was 20 mm x 0.57 = 11.40 mm.

The results in Table 7 show that the design life adopted by the ATEB [19] for the 120-mm-thick BSM base course pavement section was satisfactory because the rut depths (3.71 mm for NA and 3.10 mm for CDA) formed during the design life in the BSM base course pavement section were lower than the 11.40-mm rut-depth failure. Moreover, all the pavement section combinations of HMA thickness and BSM thickness generated rut depths smaller than those of the rut depth failures. Therefore, all the studied sections were suitable from a rutting point of view.

6. Conclusions

This study investigated the mechanical behaviour of BSM base-course pavement sections of low-volume roads made with natural aggregates and construction and demolition aggregates. In this regard, the responses at critical positions of pavement layer sections and the cumulative permanent deformation (rutting) of the BSM layers were analysed. Based on the results of this research, the following conclusions can be drawn.

- BSM base courses with NAs and with CDAs present a typical nonlinear behaviour with a resilient modulus dependency on the stresses.
- The resilient modulus is higher in cured and uncured BSM base courses with NAs. Nevertheless, the shear strength before curing is higher in the BSM base courses with CDAs and after curing it is comparable with both types of aggregates. The BSM base courses made with CDAs had less cumulative axial permanent strain ε_p (%) than the BSM base courses with NAs.
- The rutting produced during the curing period is approximately 50% of the total rutting produced

during the design life period. The total rutting produced in a BSM base course made with CDAs is lower than the total rutting produced in a BSM base course made with NAs. All the BSM base-course pavement sections were able to resist rutting during the design life period. Therefore, it is possible to use CDAs in BSM materials.

Finally, it must be noted that the present research is a first step in the numerical simulation performance prediction of BSM base courses made with CDAs and NA aggregates. The results were encouraging and showed that the BSM made with CDAs might have high potential use in road pavements. However, further investigation is necessary to assess aspects such as the BSM with CDAs cumulative permanent strain (rutting) resistance, the effect of different curing times on the mechanical performance and the cracking performance.

Acknowledgements

The authors acknowledge the funding of project BIA2016-80317-R from the Spanish Ministry of Economy and Competitiveness.

References

[1] Transportation Research Board, Asphalt Emulsion Technology, Transportation Research Circular Number E-C102, Washington DC (USA), 2006.

[2] I.N.A. Thanaya, S.E. Zoorob, J.P. Forth, A laboratory study on cold-mix, cold lay emulsion mixtures, Proc. Inst. Civ. Eng. Trans. 162 (2009) 47–55. https://doi.org/10.1680/tran.2009.162.1.47

[3] M. Limbachiya, M.S. Meddah, Y. Ouchagour, Use of recycled concrete aggregate in fly-ash concrete, Constr. Build. Mater. 27 (2012) 439–449. https://doi.org/10.1016/j.conbuildmat.2011.07.023

[4] M. Pepe, R.D. Toledo Filho, E.A.B. Koenders, E. Martinelli, Alternative processing procedures for recycled aggregates in structural concrete, Constr. Build. Mater. 69 (2014) 124–132. https://doi.org/10.1016/j.conbuildmat.2014.06.084

[5] Y.D. Wong, D.D. Sun, D. Lai, Value-added utilization of recycled concrete in hot- mix asphalt, Waste Manag. 27 (2007) 294–301. https://doi.org/10.1016/j.wasman.2006.02.001

[6] A.R. Pasandín, I. Pérez, Overview of bituminous mixtures made with recycled concrete aggregates, Constr. Build. Mater. 74 (2015) 151–161. https://doi.org/10.1016/j.conbuildmat.2014.10.035

[7] F. Lekarp, U. Isacsson, A. Dawson, State of the art. I: resilient response of unbound aggregates, J. Trans. Eng. 126 (2000) 66–75. https://doi.org/10.1061/(ASCE)0733-947X(2000)126:1(66)

[8] K.J. Jenkins, M. Yum, Cold-recycling techniques using bitumen stabilization: Where is the technology going? In: W.Steyn, J. Kim Jenkins, M. Solaimanian (eds.), ASCE Geotechnical Special Publication 191, Road Pavement Material Characterization and Rehabilitation: Selected Papers from the 2009 GeoHunan International Conference, Hunan, China, 2009, pp. 191-200. https://doi.org/10.1061/9780784410431

[9] K.J. Jenkins, F. M. Long, L.J. Ebels, Foamed bitumen mixes=shear performance? Int. J. Pavement Eng. 8 (2007) 85-98. https://doi.org/10.1080/10298430601149718

[10] L.J. Ebels, Characterisation of Material Properties and Behaviour of Cold Bituminous Mixtures for Road Pavements. PhD thesis. Stellenbosch University, South Africa, 2008.

[11] K.J. Jenkins, D.S. Collings, Mix design of bitumen-stabilised materials–South Africa and abroad.

Road Mater. Pavement. 18 (2017) 331-349. https://doi.org/10.1080/14680629.2016.1213511
[12] P. Hornych, V. Gaudefroy, J.L Geffard, S. Goyer, Study of the mechanical behaviour of gravel-emulsion using triaxial tests. In: A. Loizos, M.N Partl, T. Scarpas, I.L. Al-Qadi, (eds.), Proceedings of the 7th International RILEM Symposium on Advanced Testing and Characterization of Bituminous Materials (ATCBM09), CRC Press/Balkema, Rhodes, Greece, 2009, pp. 639-649.
[13] E. Santagata, G. Chiapinelli, P.P. Riviera, O. Baglieri, Triaxial testing for the short term evaluation of cold-recycled bituminous mixtures. Road Mater. Pavement. 11 (2010) 123-147. https://doi.org/10.1080/14680629.2010.9690263
[14] B. Gómez-Meijide, I. Pérez, Nonlinear elastic behavior of bitumen emulsion-stabilized materials with C&D waste aggregates, Constr. Build. Mater. 98 (2015) 853–863. https://doi.org/10.1016/j.conbuildmat.2015.07.004
[15] Y.H. Huang, Pavement Analysis and Design. Pearson Prentice Hall, second edition, Upper Saddle River, NJ USA, 2004.
[16] H. K. Shambara, A. Dulaimi, F. Ruddock, W. Atherton, The linear elastic analysis of cold mix asphalt by using finite element modeling, Conference Proceedings, The 2nd BUiD Doctoral Research Conference BDRC 2016, The British University in Dubai, 14th May, 2016.
[17] H. K. Shambara, F. Ruddock, W. Atherton, Predicting the rutting behaviour of natural fibre-reinforced cold mix asphalt using the finite element method. Constr. Build. Mater. 167 (2018) 907-917. https://doi.org/10.1016/j.conbuildmat.2018.02.072
[18] I. Pérez, L. Medina, L., M.A. del Val, Nonlinear elasto-plastic performance prediction of materials stabilized with bitumen emulsion in rural road pavements, Adv. Eng. Softw. 91 (2016) 69-79. https://doi.org/10.1016/j.advengsoft.2015.10.009
[19] ATEB, Technical Association of Bituminous Emulsions, Gravel-emulsion specifications. https://www.ateb.es/images/pdf/PLI_GRAVA.pdf. (Accessed 24 April 2018) (in Spanish).
[20] R.G. Hicks, Factors influencing the resilient response of granular materials. Doctoral Dissertation, University of California, Berkeley, USA, 1970.
[21] J. Uzan, M.W. Witczak, T. Scullion, R.L. Lytton, Development and validation of realistic pavement response models. Proceedings of the 7th International Conference on Asphalt Pavements. Nottingham, UK, 1992, pp. 334-350.
[22] NCHRP (National Cooperative Highway Research Program), Guide for Mechanistic-Empirical Design of New and Rehabilitated Pavement Structures, Part 2 Design Inputs, Final Report NCHRP 1-37A, 2004.
[23] M.R. Thompson, R.P. Elliot, Illi-Pave-Based Response Algorithms for Design of Conventional Flexible Pavements. Transp. Res. Record 1043 (1985) 50-57.
[24] Itasca Consulting Group, Inc. FLAC3D (Fast Lagrangian Analysis of Continua in 3 Dimensions), Version 3.10, User's manual, Minneapolis, MN, 2006.
[25] L. Medina, I. Pérez, R. Crespo, Structural verification of roadbed sections according to the Spanish road design manual 6.1 and 6.2 I.C. Revista de Obras Públicas 149 (3417) (2002) 35-52 (in Spanish).
[26] J.J.E. Liebenberg, A.T. Visser, Towards a mechanistic structural design procedure for emulsion-treated base layers. J. S. Afr. Inst. Civ. Eng. 46 (2004) 2-8.
[27] B.C. Roos, A design function for Bitumen Stabilised Material performance based on laboratory and filed evaluation. PhD thesis. Stellenbosch University, South Africa, 2018.